AIM and ELF Analyses and Gas-Phase Acidities of Some Main-Group Oxyacids (H_zXO_4, X = Cl, S, P, Si and Br, Se, As, Ge)

Jean-François Boily*

Institut für Mineralogie und Petrographie, Swiss Federal Institute of Technology (ETH) Zürich, Sonneggstr. 5, CH-8092 Zürich, Switzerland

Received: September 6, 2002; In Final Form: March 17, 2003

Oxyacids of the form H_zXO_4 (X = Cl, S, P, Si and Br, Se, As, Ge) were investigated with (1) the theories of atoms in molecules (AIM) and the electron localization function (ELF) at the B3LYP/6-311++G(3df,pd) level and with (2) G2 calculations. AIM and ELF analyses classify X−O bonds of 3rd-row oxyacids as σ-bonded shared interactions with ELF disynaptic basin populations ranging from 1.39 to 2.17*e*. Those of 4th-row oxyacids have no ELF disynaptic basin populations, save X−OH bonds with smaller values ranging from 0.67 to only 1.07*e*. Both bonds are classified as mostly σ-bonded closed-shelled interactions. The oxygen valence shell electron population in 3rd-row oxyacids range from 5.76 to 6.12*e* and from 7.86 to 7.96*e* in their 4th-row counterparts, and all OH disynaptic basin populations range from 1.70 to 1.79*e*. These populations have no correlation with the wide range of acid strengths of the oxyacids. The concept of underbonding, whereby the oxygen valence shell electron population is said to be proportional to acidity, therefore does not hold from this perspective. Acidity is better rationalized in terms of the electrostatic potential at H sites.

1. Introduction

Intramolecular distributions of electrons can provide clues on the nature of chemical bonds and on the reactivity of moieties. The concept of partial charge has notably prevailed in rationalizing chemical reactions. Charge distributions based on the concept of bond valences[1,2] have, for instance, been used to rationalize trends in acidities of aqueous monomers[3] and, more recently, relationships between modes of oxyacid coordination at metal (hydr)oxide/water interfaces and proton exchange.[4] In this approach a central cation is said to distribute its charge either equally (Pauling bond valence[1]) or unequally (actual bond valence[2]) to its coordinated ligands. The degree of "underbonding" of a coordinating ligand, determined from the residual charge (i.e., the formal charge of the moiety minus the charge contribution of the cation), is then said to be indicative of the reactivity of the ligand. In this context, a basic moiety with a small residual charge would, for example, be more acidic than one with a larger charge.

A more rigorous approach involves a quantum chemical investigation of molecular geometries and their associated charge distributions. Analyses of the topology of the electron density obtained from theoretical wave functions can be carried out with Bader's theory of atoms in molecules (AIM).[5] This approach can give information on the nature of bonds, on the number and position of (non)bonding electrons, and on atomic electronic populations. Silvi and Savin's[6] topological analysis of the Becke−Edgecombe electron localization function[7] (ELF) also retrieves populations of electrons localized in atomic cores and in (non)bonding valence shells of atoms. Both approaches provide an explicit notion of the (statistical) distribution of electrons within molecules and even atoms (for ELF).

In this study, oxyacids of the form H_zXO_4 (X = Si(IV), P(V), S(VI), Cl(VII) and Ge(IV), As(V), Se(VI), Br(VII)) are analyzed with AIM and ELF to document the changes in the nature of X−O bonds and charge distributions upon the protonation of their conjugate bases. This study builds upon a previous study[8] reporting the nature of X−O bonds in XO_4 main-group oxyanions and a variety of charge distributions.[5,9,10] One important goal consists of testing the concept of underbonding as a rationalizing concept for acidity using results from gas-phase G2[11] calculations and aqueous-phase pK_a's. While other thermochemical calculations[12−14] have already outlined some salient trends in oxyacid acidity, topological analyses of the electron density have not been considered in this context. These results may notably impact the application of the concept of underbonding in predicting the acidity of basic moieties, such as it has been done for metal (hydr)oxide surface functional groups.[15]

2. Methods

2.1. Topological Analyses. *2.1.1. AIM.* The theory of AIM[5] reveals insightful information on the nature of bonds. A (3,−1) critical point[5] of the electron density, $\rho(r)$, located between two atomic centers denotes the presence of a bond. Charge density at such a point is referred as $\rho(r_c)$. Topologically, this corresponds to a point in real space where the gradient of $\rho(r_c)$, $\nabla\rho(r_c)$, is zero and where the curvature of $\rho(r_c)$, expressed through three eigenvalues of the diagonalized Hessian of $\rho(r_c)$, is positive ($\lambda_3 = \partial^2\rho(r_c)/\partial z^2$) for an eigenvector linking two atomic centers, and negative ($\lambda_1 = \partial^2\rho(r_c)/\partial x^2$; $\lambda_2 = \partial^2\rho(r_c)/\partial y^2$) for the two others perpendicular to it. Unequal values of λ_1 and λ_2 at (3,−1) bond critical points denote an anisotropic spread of electrons quantified through the concept of ellipticity:[5]

$$\epsilon = \lambda_1/\lambda_2 - 1 \qquad (1)$$

(with $\lambda_1 > \lambda_2$) where values of $\epsilon \gg 1$ can be indicative of π bonding. A bond path[5] is defined as a curve linking two atomic centers through a trajectory where values of $\rho(r)$ are the largest

* Phone: +41 1 632 6394. Fax: +41 1 632 1088. E-mail: boily@erdw.ethz.ch.

10.1021/jp0269221 CCC: $25.00
Published on Web 05/03/2003

possible. A chemical bond is then said to result from the competition of the expansion of $\rho(r)$ toward respective atomic centers and the contraction of $\rho(r)$ toward the bond path. If the former dominates the ratios $|\lambda_1|/\lambda_3$ and $|\lambda_2|/\lambda_3$ are < 1, while if the latter dominates, the ratios are >1. The Laplacian of $\rho(r_c)$, $\nabla^2\rho(r_c)$, measures the dominant effect with

$$\nabla^2\rho(r_c) = \lambda_1 + \lambda_2 + \lambda_3 \quad (2)$$

It is also related to the (positive) kinetic energy density, $G(r_c)$, and to the (negative) electronic potential energy, $V(r_c)$, with

$$^1/_4\nabla^2\rho(r_c) = 2G(r_c) + V(r_c) \quad (3)$$

expressed in atomic units. Thus when $\nabla^2\rho(r_c) < 0$ charge is locally concentrated and possesses an absolute value of $V(r_c)$ that is more than twice that of $G(r_c)$. Conversely, when $\nabla^2\rho(r_c) > 0$, charge is locally depleted. Typically, a shared interaction of electrons (covalent, dative, or metallic bonds) is identified with a (3,−1) bond critical point of a large $\rho(r_c)$, a large and negative $\nabla^2\rho(r_c)$, and ratios of $G(r_c)/\rho(r_c) < 1, |\lambda_1|/\lambda_3 > 1$ and $|\lambda_2|/\lambda_3 > 1$. A closed-shell interaction of electrons (ionic, van der Waals, or hydrogen bonds) is identified with a small $\rho(r_c)$, a large and positive $\nabla^2\rho(r_c)$, and ratios of $G(r_c)/\rho(r_c) > 1, |\lambda_1|/\lambda_3 < 1$, and $|\lambda_2|/\lambda_3 < 1$. Also, the local electronic energy density, $E_e(r_c)$:

$$E_e(r_c) = G(r_c) + V(r_c) \quad (4)$$

denotes a stabilizing accumulation of charge if $E_e(r_c) < 0$ and a destabilizing accumulation of charge if $E_e(r_c) > 0$.

Last, a (3,−3) critical point[5] in $-\nabla^2\rho(r)$ corresponds to local concentration of charge, or a valence shell charge concentration (VSCC). These points are of interest as these can reveal loci of local charge concentration, akin to Lewis' lone pairs.[16−17]

2.1.2. ELF. The ELF[7] has been suggested to be a measure of the Pauli repulsion:[7,18]

$$\eta(r) = \frac{1}{1 + \left(\frac{D_\sigma(r)}{D_\sigma{}^0(r)}\right)^2} \quad (5)$$

where $D_\sigma(r)$ is the local excess kinetic energy density due to Pauli repulsion and $D_\sigma{}^0(r)$ is the kinetic energy density of a reference homogeneous electron gas of the same electron density, a value that essentially acts as a renormalization factor. Values of $\eta(r)$ thus range from 0 to 1 with larger values denoting larger electron localization, i.e., a higher probability of finding electrons alone or in pairs of antiparallel spin. The gradient field of the ELF, $\nabla\eta(r)$, can be also used to partition space into localization basins.[6] Each of these basins contains a (3,−3) critical point of $\eta(r)$, also referred to as an attractor, which may or may not contain an atomic center. Basins are visualized for any given isodensity value of $\eta(r) = f$, which in turn encompass regions of $\eta(r) \geq f \leq 1$.

Basins are classified as either (1) core basins, C(atom), encompassing a nucleus ($Z > 2$) and core electrons, or as (2) valence basins, V(atom(s)), encompassing valence shell electrons.[19] Valence basins are furthermore categorized by their synaptic order which refers to the number of core basins with which they share a common boundary. A monosynaptic basin, e.g., V(X), encompasses lone pairs (not necessarily exactly 2*e*) while a polysynaptic basin, e.g., V(X, O_1,..., O_n), encompasses electrons involved in bi- or polycentric bonds. The presence of a di- or polysynaptic basin is indicative of a shared interaction of electrons (covalent, dative, or metallic bonds), while its absence denotes a closed-shell interaction (ionic, van der Waals or hydrogen bond). If a valence basin contains one proton, its synaptic order is increased by one such that H_2O, for example, has two V(O,H) disynaptic basins, in addition to one C(O) and two V(O) basins (lone pairs).[20]

The electronic population of a synaptic basin, $\bar{N}$, is obtained as the integral of the one-electron density of the basin.[21] The variance of the basin population, $\bar{N}$, represents the quantum mechanical uncertainty on $\bar{N}$ and is related to the delocalization of electrons.[21] The relative fluctuation of a basin:[5]

$$\lambda = \frac{\sigma^2(\bar{N})}{\bar{N}} \quad (6)$$

is a good measure of electron delocalization where values greater than 0.45 typically denote a significant degree of delocalization.[19]

2.2. Computational Details. The geometries of all oxyacids were fully optimized from different starting geometries with B3LYP[22] using the Cartesian 6-311++G(3df,pd) basis set with the program Gaussian98.[23] Additional calculations were carried out with the Cartesian basis sets 6-31G, 6-31++G(d,p), 6-311++G(d,p), 6-311G(2d,pd), and 6-311+G(3df,pd) for H_zSiO_4 oxyacids, mostly to investigate the effects of diffuse and polarization schemes on the outcome of the interpretations. Frequency calculations at the B3LYP/6-311++G(3df,pd) level were carried out on all oxyacids to confirm that the stationary points correspond to minima on potential energy surfaces. The stability of the wave function[24,25] obtained at the same level of theory was also confirmed for all oxyacids. Gaussian98-formatted wave function (.wfn) files were then generated for AIM and ELF topological analyses of the electron density. Last, the electrostatic potential at nucleic positions was determined using the PRISM algorithm,[26] as implemented in Gaussian98.

The program MORPHY98[27] was used for all AIM analyses to obtain values of (1) $\rho(r_c)$, (2) $\nabla^2\rho(r_c)$, (3) λ_1, λ_2, and λ_3, and (4) $G(r_c)$. The program TopMoD[20] was used for ELF analyses to identify synaptic basins and their respective orders and to calculate (1) $\bar{N}$, (2) $\sigma^2\bar{N}$, and (3) λ on a working grid of 0.1 au. Visual rendering of synaptic basins are carried out using .stf files of TopMod.[28] MORPHY98[27] is also used to calculate $\eta(r)$ in predefined trajectories in some oxyacids.

The gas-phase enthalpy of acidity,[28−29] $\Delta_{acid(g)}H_o$, for the reaction at 298.15 K:

$$HA^0 \rightleftharpoons H^+ + A^{1-} \quad (7)$$

where HA is a neutrally-charged acid and A^{1-} its conjugate base, is obtained from G2[30] calculations of HA^0 and A^{1-} with the program Gaussian98.[23] This value includes zero-point-vibrational-energy corrections as well as a thermal correction to the electronic energies due to translational, rotational, and vibrational contributions. The same is applied to quantify the acidity of singly charged anions.

3. Results and Discussion

3.1. Geometry Optimization. Protonation exerts important changes in X−O(H) bond lengths and the geometry of oxyacids, while O−H bond lengths are invariably in the range 0.961−0.974 Å (Tables 1 and 2). Moreover, all X−O bond lengths reported in this study are close to the range of experimental solid-state values.[31]

Protonation breaks the T_d symmetry of XO_4 anions to yield three different X−O bond lengths in HXO_4 (Figure 1). The

TABLE 1: Bond Lengths and AIM Analyses of X−O(H) Bonds (B3LYP/6-311++G(3df,pd))

		r (Å)[a]	ρ (r_c)[b]	$\nabla^2\rho$ (r_c)[c]	λ_1/λ_3[d]	ϵ[e]	$G(\rho(r_c))/\rho(r_c)$[f]	E_e (r_c)[g]
$HClO_4^0$	Cl−O_I	1.412	0.402	−0.633	0.943	0.057	1.259	−0.67
	Cl−O_{II}	1.421	0.396	−0.701	1.062	0.071	1.279	−0.68
	Cl−OH	1.658	0.254	−0.363	0.818	0.075	0.546	−0.23
HSO_4^{1-}	S−O_I	1.449	0.312	0.642	0.331	0.046	1.797	−0.40
	S−O_{II}	1.458	0.307	0.581	0.341	0.055	1.750	−0.39
	S−OH	1.675	0.202	−0.239	0.803	0.020	0.806	−0.22
HPO_4^{2-}	P−O_{II}	1.540	0.217	0.853	0.251	0.031	1.809	−0.18
	P−O_I	1.525	0.223	0.926	0.246	0.042	1.870	−0.19
	P−OH	1.755	0.135	0.223	0.334	0.045	1.134	−0.10
$HSiO_4^{3-}$	Si−O_{II}	1.663	0.138	0.734	0.204	0.015	1.739	−0.06
	Si−O_I	1.638	0.146	0.813	0.202	0.033	1.813	−0.06
	Si−OH	1.874	0.082	0.299	0.225	0.021	1.246	−0.03
$HBrO_4^0$	Br−O_I	1.593	0.284	0.024	0.494	0.030	1.078	−0.30
	Br−O_{II}	1.600	0.279	0.025	0.494	0.036	1.063	−0.29
	Br−OH	1.800	0.189	0.008	0.513	0.085	0.702	−0.13
$HSeO_4^{1-}$	Se−O_{II}	1.635	0.241	0.273	0.370	0.026	1.221	−0.23
	Se−O_I	1.624	0.246	0.302	0.364	0.032	1.254	−0.23
	Se−OH	1.827	0.161	0.096	0.433	0.074	0.826	−0.11
$HAsO_4^{2-}$	As−O_{II}	1.696	0.193	0.492	0.275	0.018	1.338	−0.14
	As−O_I	1.682	0.199	0.528	0.271	0.025	1.374	−0.14
	As−OH	1.902	0.122	0.196	1.055	0.055	0.941	−0.07
$HGeO_4^{3-}$	Ge−O_{II}	1.787	0.145	0.516	0.225	0.008	1.357	−0.07
	Ge−O_I	1.770	0.150	0.552	0.224	0.018	1.391	−0.07
	Ge−OH	2.006	0.087	0.218	0.259	0.035	1.001	−0.03
$H_2SO_4^0$	S−O	1.421	0.329	0.873	0.293	0.010	1.963	−0.43
	S−OH	1.594	0.238	−0.058	0.558	0.082	1.122	−0.28
$H_2PO_4^{1-}$	P−O	1.489	0.242	1.136	0.227	0.007	2.031	−0.21
	P−OH	1.657	0.166	0.450	0.296	0.066	1.421	−0.12
$H_2SiO_4^{2-}$	Si−O	1.596	0.163	0.981	0.193	0.012	1.957	−0.07
	Si−OH	1.769	0.105	0.481	0.221	0.056	1.486	−0.04
$H_2SeO_4^0$	Se−O	1.597	0.259	0.370	0.341	0.004	1.330	−0.25
	Se−OH	1.757	0.187	0.112	0.440	0.098	0.935	−0.15
$H_2AsO_4^{1-}$	As−O	1.646	0.215	0.635	0.256	0.005	1.471	−0.16
	As−OH	1.811	0.149	0.294	0.315	0.078	1.108	−0.09
$H_2GeO_4^{2-}$	Ge−O	1.725	0.167	0.671	0.214	0.005	1.498	−0.08
	Ge−OH	1.907	0.109	0.330	1.062	0.062	1.169	−0.05
$H_3PO_4^0$	P−O	1.463	0.256	1.318	0.213	0.001	2.163	−0.22
	P−OH	1.590	0.192	0.650	0.282	0.081	1.619	−0.15
$H_3SiO_4^{1-}$	Si−O	1.559	0.178	1.152	0.185	0.001	2.094	−0.09
	Si−OH	1.690	0.127	0.669	0.220	0.077	1.675	−0.05
$H_3AsO_4^0$	As−O	1.620	0.227	0.719	0.246	0.001	1.542	−0.17
	As−OH	1.774	0.173	0.404	0.300	0.082	1.244	−0.11
$H_3GeO_4^{1-}$	Ge−O	1.688	0.182	0.780	0.207	0.000	1.590	−0.09
	Ge−OH	1.832	0.133	0.479	0.236	0.071	1.336	−0.06
$H_4SiO_4^0$	Si−OH	1.635	0.146	0.838	0.214	0.088	1.832	−0.06
$H_4GeO_4^0$	Ge−OH	1.766	0.152	0.611	0.227	0.077	1.466	−0.07

[a] Bond length (Å). [b] Electron density. [c] Laplacian of the charge density. [d] Ratio of the eigenvalues of the Hessian of $\rho(r_c)$ perpendicular and parallel to X−O. [e] Ellipticity. [f] Ratio of the electronic kinetic energy density and the electron density. [g] Local electronic energy density. All AIM values are reported in atomic units. See entire caption of Figure 1.

X−OH bond (i.e., protonated oxygen) elongates 0.16−0.20 Å, while the three remaining X−O bonds (i.e., unprotonated oxygens) contract 0.029−0.063 Å relative to their respective XO_4 bases. The proton in HSO_4^{1-}, $HClO_4^0$, and $HBrO_4^0$ is oriented mid-way between two adjacent unprotonated oxygens (Figure 1). These two oxygens (O_I) have also slightly longer bond lengths than the remaining one. The proton in all other HXO_4 molecules is oriented directly toward only one unprotonated oxygen. This oxygen (O_{II}) has then a slightly longer bond than the two remaining ones.

The H_2XO_4 molecules have both protons oriented toward a different unprotonated oxygen. In this protonation step and in all subsequent ones X−OH bonds undergo a contraction relative to their conjugate bases due to the reduction in the formal negative charge of the molecule. In H_2XO_4 molecules the contraction is of 0.081−0.103 Å relative to HXO_4. X−OH bond lengths are nonetheless always longer than X−O bonds. The two remaining unprotonated X−O bonds contract further 0.028−0.067 Å relative to HXO_4 oxyanions due to the combined effects of reduced formal charge and protonation on adjacent O atoms.

TABLE 2: Bond Lengths and AIM Analyses of O−H Bonds (B3LYP/6-311++G(3df,pd))

	r(Å)[a]	$\rho(r_c)$[b]	$\nabla^2\rho(r_c)$[c]	λ_1/λ_3[d]	ϵ[e]	$G(\rho(r_c))/\rho(r_c)$[f]	$E_e(r_c)$[g]
$HClO_4^0$	0.974	0.353	−2.500	1.731	0.016	0.188	−0.69
HSO_4^{1-}	0.965	0.364	−2.498	1.741	0.012	0.214	−0.70
HPO_4^{2-}	0.963	0.367	−2.484	1.735	0.011	0.231	−0.71
$HSiO_4^{3-}$	0.966	0.362	−2.419	1.715	0.005	0.240	−0.69
$HBrO_4^0$	0.975	0.351	−2.475	1.725	0.012	0.192	−0.69
$HSeO_4^{1-}$	0.967	0.361	−2.495	1.741	0.013	0.214	−0.70
$HAsO_4^{2-}$	0.966	0.363	−2.435	1.733	0.016	0.233	−0.69
$HGeO_4^{3-}$	0.968	0.360	−2.382	1.712	0.005	0.242	−0.68
$H_2SO_4^0$	0.970	0.354	−2.532	1.705	0.012	0.188	−0.70
$H_2PO_4^{1-}$	0.963	0.364	−2.519	1.734	0.018	0.215	−0.71
$H_2SiO_4^{2-}$	0.963	0.365	−2.445	1.725	0.007	0.236	−0.70
$H_2SeO_4^0$	0.972	0.352	−2.495	1.713	0.012	0.194	−0.69
$H_2AsO_4^{1-}$	0.966	0.361	−2.476	1.736	0.010	0.218	−0.70
$H_2GeO_4^{2-}$	0.965	0.363	−2.402	1.721	0.007	0.238	−0.69
$H_3PO_4^0$	0.965	0.356	−2.541	1.692	0.007	0.195	−0.70
$H_3SiO_4^{1-}$	0.961	0.364	−2.486	1.728	0.006	0.224	−0.70
$H_3AsO_4^0$	0.967	0.356	−2.515	1.710	0.009	0.200	−0.70
$H_3GeO_4^{1-}$	0.963	0.364	−2.465	1.734	0.008	0.227	−0.70
$H_4SiO_4^0$	0.960	0.361	−2.551	1.694	0.004	0.205	−0.71
$H_4GeO_4^0$	0.964	0.359	−2.513	1.714	0.007	0.208	−0.70

[a] Bond length (Å). [b] Electron density. [c] Laplacian of the charge density. [d] Ratio of the eigenvalues of the Hessian of $\rho(r_c)$ perpendicular and parallel to X−O. [e] Ellipticity. [f] Ratio of the electronic kinetic energy density and the electron density. [g] Local electronic energy density. All AIM values are reported in atomic units.

The X−OH bonds in H_3XO_4 molecules are contracted by 0.067−0.085 Å and X−O contracted by 0.026−0.037 Å relative to H_2XO_4 oxyanions. The shortest P−O, Si−O, As−O, and Ge−O bonds also occur in these molecules.

The H_4XO_4 molecules have protons oriented toward what could be seen as the nonbonding orbitals of neighboring protonated oxygens. The newly protonated X−OH bond elongates 0.076−0.077 Å, while the remaining X−OH bonds contract 0.055−0.058 Å relative to H_3XO_4.

3.2. The Nature of X−O(H) Bonds. *AIM Analyses.* The properties of (3,−1) bond critical points of X−O(H) bonds calculated at the B3LYP/6-311++G(3df,pd) level are reported in Table 1. All X−O(H) bond critical points display a significant concentration of electrons with $\rho(r_c)$ ranging from 0.138 to 0.400 au for H_zSiO_4 to $HClO_4^0$, and from 0.145 to 0.284 au for H_zGeO_4 to $HBrO_4^0$, respectively. These values are close to those of XO_4 oxyanions with 0.12 to 0.37 au for SiO_4^{4-} to ClO_4^{1-}, and from 0.14 to 0.27 au for GeO_4^{4-} to BrO_4^{1-}, respectively.[8] A closer inspection, however, reveals additional insight into the nature of these values. As noted in the previous section, X−O bonds undergo a slight contraction at each protonation step. Two unprotonated oxygens of perchlorate, for instance, undergo a contraction in bond length of 0.037 Å at the first protonation step and display a concomitant increase in $\rho(r_c)$ from 0.37 to 0.396 au. Figure 2a,b illustrates the resulting power or exponential relationships between X−O(H) bond lengths and $\rho(r_c)$, in agreement with similar relationships already shown in previous studies.[32−36] In fact, the results of Gibbs et al.[32,34] on neutrally-charged Si(IV) and Ge(IV) hydroxyacids (B3LYP/6-311G(2d,p)) are in good agreement with their charged monomeric counterparts considered in this study. This result also suggests that while it is possible that negatively charged gas-phase molecules yield exaggerated calculated longer bonds (thereby increasing the closed-shell nature of an interaction

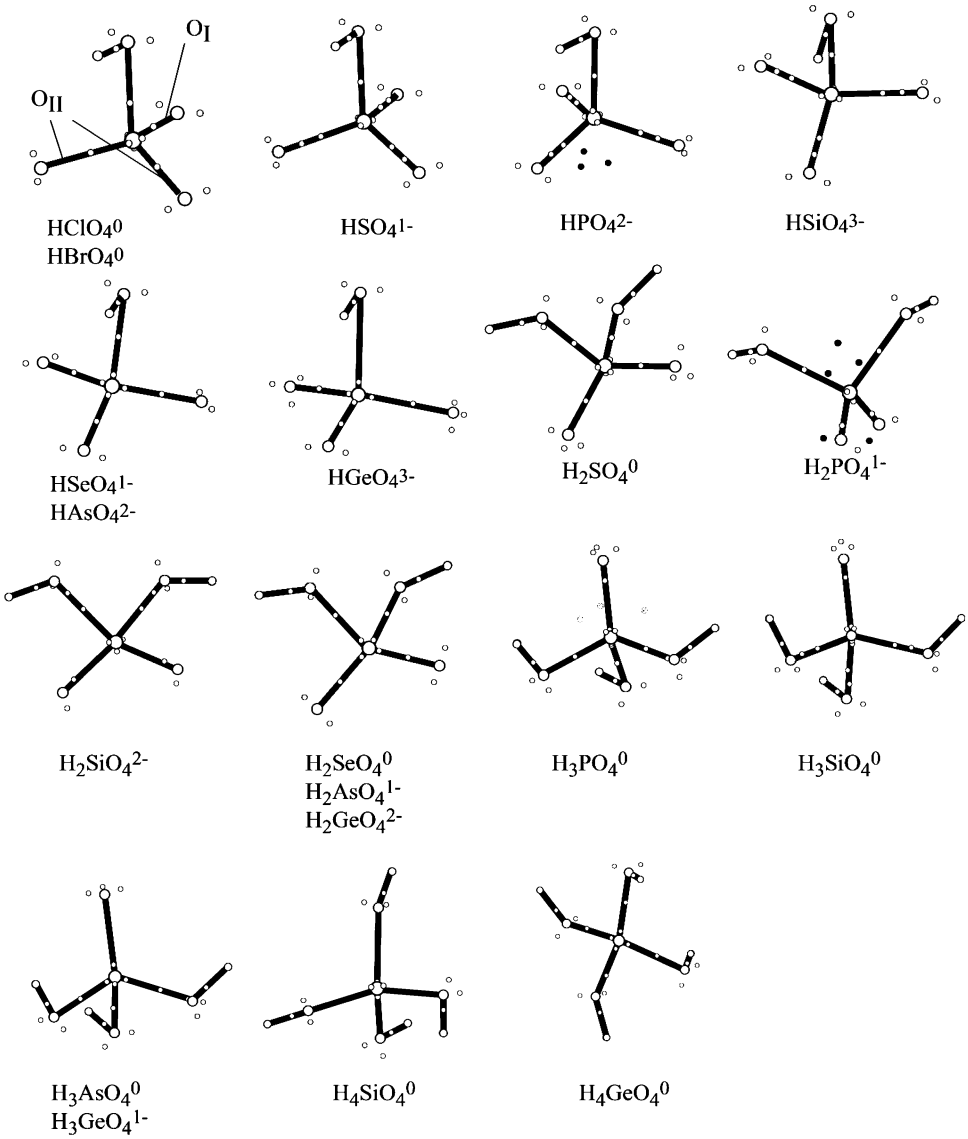

Figure 1. Optimized geometries of oxyacids considered in this study. The smallest circles (open, gray, and black) are loci of VSCC determined by (3,−3) critical points of $-\nabla^2\rho(r)$. X−O bonds in HXO_4 are denoted as $X-O_I$ and $X-O_{II}$, where the former denotes that only one bond has this specific distance and the latter denotes that there are two bonds with another specific distance.

through a redistribution of electrons in oxygen valence shells), the trends in X−O bonds outlined here and in a previous publication[8] are chiefly due to the nature of X.

The effects of basis sets on the AIM analyses are shown for H_zSiO_4 oxyanions in Figure 2c. The results show larger basis sets to yield larger values of $\rho(r_c)$. Basis sets of triple-ζ quality yield concordant results as long as diffuse and polarization functions are used for all elements. The remaining analyses are therefore based on the results of the calculations with the 6-311++G(3df,dp) basis set.

Figure 3a,b shows the relationship between $\nabla^2\rho(r_c)$ and X−O(H) bond lengths, which are also similar to those of Si(IV) and Ge(IV) hydroxyacids reported by Gibbs et al.[32,34] Positive (negative) values of $\nabla^2\rho(r_c)$ decrease (increase) and appear to converge toward values intermediate to 0 and 0.2 at the largest X−O(H) bond length considered in this study. The large negative values of Cl also show a minimum at a bond length of 1.45 Å and a strong increase at smaller bond lengths. Despite the general increase of $\nabla^2\rho(r_c)$ with increasing $\rho(r_c)$ the overall energy of bond critical point electrons decreases, as shown in Figure 3c,d. In other words, the decrease in $V(r_c)$ with decreasing bond length is more important than the increase in $G(r_c)$ (eq 4), giving rise to a more stable accumulation of electrons at the bond critical point at small X−O bond lengths. At even smaller bond lengths, nucleic repulsion should give rise to a reversal in this trend.

The (3,−1) bond critical point properties of the oxyacids (Table 1) thus show the nature of X−O interactions to remain similar to those of XO_4 oxyanions. Indeed, the significant values of $\rho(r_c)$ along with values of $\nabla^2\rho(r_c) > 0$, $\lambda_1/\lambda_3 < 1$, $G(\rho(r_c))/\rho(r_c) > 1$, and $E_e(r_c) < 0$ point to an interaction intermediate to closed-shell and shared nature. $HClO_4^0$ remains an exception, where its bond critical point properties suggest shared interactions. The nature of the X−OH bond is also similar to that of X−O bonds, although the longer X−OH bond, likely resulting from X−H repulsion, yields smaller values of $\rho(r_c)$, ranging from 0.082 to only 0.254 au for H_zSiO_4 to $HClO_4^0$, and from 0.087 to only 0.189 au for H_zGeO_4 to $HBrO_4^0$. Values of $\nabla^2\rho(r_c)$ and $G(\rho(r_c))/\rho(r_c)$ are also smaller than those of X−O bonds in XO_4 and values of $\nabla^2\rho(r_c)$ are even negative in HSO_4^{1-} and $H_2SO_4^0$. Although this would point to a smaller kinetic energy density for (3,−1) bond critical point electrons, values of $E_e(r_c)$ are not as negative as those of X−O bonds.

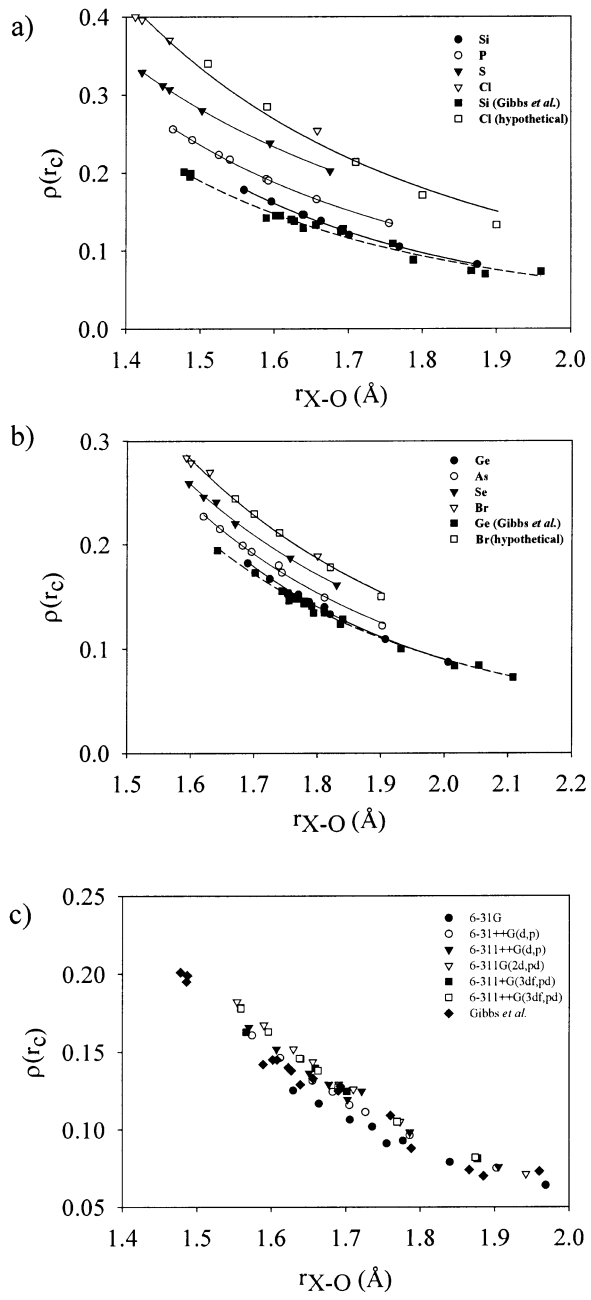

Figure 2. Electron density (in atomic units) at the (3,−1) bond critical point as a function of X−O bond lengths for (a) 3rd- and (b) 4th-row oxyacids (Table 1) and oxyanions[10] obtained at the B3LYP/6-311++G(3df,dp) level, and (c) H_zSiO_4 oxyacids ($z = 0$ to 4) obtained with B3LYP and different basis sets. The data for Cl and Br oxyacids were augmented by additional calculations on XO_4 oxyanions at various hypothetical X−O bond lengths. The data of Gibbs et al.[32,34] for neutrally-charged Si and Ge hydroxyacids are also shown for comparison.

Last, protonation also induces small increases in values of ellipticity in both X−O and X−OH bonds, not larger than $\epsilon = 0.098$. Such values, however, only suggest small asymmetric spreads of electrons in the two planes perpendicular to the bond path, that are at any rate not deemed to be physically significant.

ELF Analysis. The results of the ELF analyses at the B3LYP/6-311++G(3df,pd) level, reported in Table 3, provide further insight into the results of the AIM analysis. Examples of typical localization domains found in the oxyacids are shown in Figure 4. Third-row oxyacids possess one large V(X,O(H)) disynaptic basin per X−O(H) bond with populations ranging from 1.39 to 2.17*e*, which are also power or exponential functions of X−O bond lengths (Figure 5a). In contrast, most 4th-row oxyacids possess small disynaptic basin populations only in X−OH bonds, with values of $\bar{N}$ ranging from 0.65 to only 1.07*e*. ELF therefore classifies 3rd-row oxyacids as shared interactions and their 4th-row counterparts as mostly closed-shell. This result is also relatively insensitive to the choice of basis set, with the notable exception of the small 6-31G basis set which hardly recovers V(X,O(H)) basins (Figure 5b). All basis sets recover C(X) and C(O) core populations close to their respective noble gas configuration with B3LYP/6-311++G(3df,pd) values of 2.04−2.07*e* ($\lambda = 0.17$) for O, 10.01−10.05*e* ($\lambda = 0.04-0.06$) for 3rd-row elements, and 27.78−27.85*e* ($\lambda = 0.04$) for 4th-row elements. Deviations from the exact noble gas core populations have already been ascribed to some partial mixing of valence shell electrons with the core of O and 3rd-row elements and of the opposite in 4th-row elements.[21,37]

Monosynaptic basins of unprotonated oxygens, V(O), range from 5.76 to 6.12*e* (ca. 3*e* pairs) in 3rd-row oxyacids, and from 7.86 to 7.96*e* (ca. 4*e* pairs) in 4th-row oxyacids. These V(O) basins are, in fact, superbasins encompassing up to three highly correlated and delocalized ($\lambda = 0.43-0.55$) sub-basins whose (3,−3) critical points of $\eta(r)$ are coordinately close to those of $-\nabla^2\rho(r)$ (Figure 1). V(O) superbasins in unprotonated oxygens of most 3rd-row oxyacids possess two V(O) sub-basins of roughly 2.8−2.9*e* and 3.2−3.3*e*, while those of their 4th-row counterparts have larger values of about 3.7−3.9*e* and 4.2−4.3*e* as a result of the absence of V(X,O) basins. Some exceptions include $H_2PO_4^{1-}$ and $H_2SiO_4^{2-}$, which have only one $\eta(r)$ attractor per O, and $H_2SO_4^0$ and $HGeO_4^{3-}$, which have three. As all XO_4 oxyanions possess three V(O) sub-basins per oxygen, protonation tends to reduce the number of V(O) sub-basins without, however, dramatically affecting the overall superbasin population.

V(O) superbasins of protonated oxygens have smaller electronic populations of 4.36−4.89*e* in 3rd-row oxyacids and of 5.35−6.26*e* in their 4th-row counterparts as a result of the presence of the V(O,H) basin, to be discussed in Section 3.3. These two V(O) superbasins possess two sub-basins of equal electronic population of about 2.4*e* each in 3rd-row oxyacids and up to 3.1*e* each in 4th-row oxyacids.

Valence Shell Charge Concentration (VSCC). The relative positions of VSCC in the different oxyacids and their conjugate bases along with the ELF population analysis provide further clues on the nature of the X−O(H) bonds. Most VSCC shown in Figure 1 are coordinately close to (3,−3) critical points of $\eta(r)$, i.e., close to V(X,O(H)) basins along a bond path and V(O) basins near oxygens. All VSCC along bond paths of 3rd-row oxyacids possess large values of $\rho(r)$, negative to neutral values of $\nabla^2\rho(r)$ and tend to be spatially closer to X in the expected order of electronegativity, as also noted for oxyanions.[8] As the population of V(X,O(H)) basins does not exceed 2*e* except in X−O bonds of $H_3SiO_4^{1-}$ and $H_3PO_4^{\circ}$, 3rd-row X−O bonds can be mostly described as polarized shared σ bonds. Those in 4th-row oxyacids are rather closed-shell σ bonds. The reduction in the number of V(O) sub-basins and VSCC from three in XO_4 to two in most oxyacids is also accompanied by a slight migration of these points away from the bond path. Indeed, the angles $\angle$ X−O−VSCC of 98−114° in XO_4 increase about 1−5° at each protonation step to $H_4XO_4^0$, suggesting the absence of π back-bonding. X−O bonds in HSO_4^{1-}, HPO_4^{2-}, $HSiO_4^{3-}$ and X−OH bonds in $H_2SiO_4^{2-}$, $H_3SiO_4^{1-}$ possess an additional

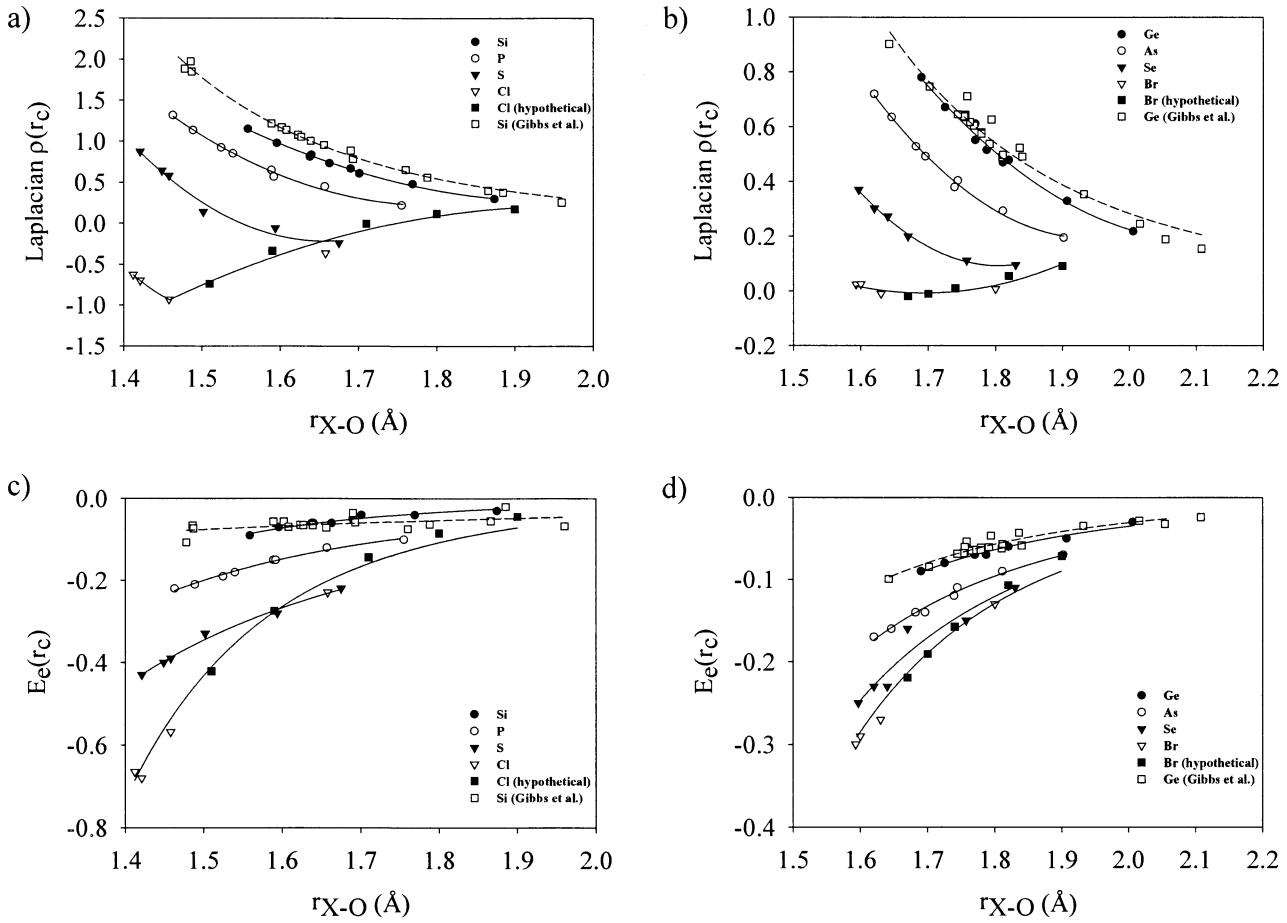

Figure 3. Laplacian of $\rho(r_c)$ and local electronic energy density (in atomic units) at (3,−1) bond critical points for (a,c) 3rd- and (b,d) 4th-row oxyacids (Table 1) and oxyanions[10] as a function of X−O bond lengths. All data are obtained at the B3LYP/6-311++G(3df,pd) level. The data of Gibbs et al.[32,34] for neutrally-charged Si and Ge hydroxyacids are also shown for comparison.

TABLE 3: ELF Synaptic Basin Population ($\bar{N}$) and Relative Fluctuation, (λ) (B3LYP/6-311++G(3df,pd)), $\bar{N}$ (λ)[a]

	C(X)	C(O)	V(X,O)	V(X,O)	V(X,OH)[b]	V(O,H)[a]	V(O)	V(O)	V(OH)[b]
$HClO_4^0$	10.03 (0.06)	2.05 (0.17)	1.93 (0.66)	1.93 (0.66)	1.40 (0.70)	1.79 (0.48)	6.00 (0.25)	5.96 (0.25)	4.87 (0.32)
HSO_4^{1-}	10.01 (0.05)	2.06 (0.17)	1.90 (0.65)	1.83 (0.65)	1.41 (0.68)	1.77 (0.49)	6.07 (0.24)	6.01 (0.24)	4.80 (0.32)
HPO_4^{2-}	10.03 (0.05)	2.06 (0.17)	1.83 (0.64)	1.72 (0.65)	1.43 (0.65)	1.72 (0.50)	6.07 (0.23)	6.08 (0.24)	4.83 (0.32)
$HSiO_4^{3-}$	10.04 (0.04)	2.06 (0.17)	1.78 (0.63)	1.76 (0.63)	1.39 (0.66)	1.74 (0.51)	6.11 (0.23)	6.10 (0.23)	4.89 (0.32)
$H_2SO_4^0$	10.02 (0.05)	2.06 (0.17)	2.04 (0.64)		1.52 (0.66)	1.77 (0.48)	5.89 (0.25)		4.65 (0.34)
$H_2PO_4^{1-}$	10.03 (0.05)	2.05 (0.17)	2.03 (0.63)		1.60 (0.63)	1.75 (0.49)	5.85 (0.24)		4.65 (0.34)
$H_2SiO_4^{2-}$	10.05 (0.04)	2.04 (0.17)	1.98 (0.61)		1.63 (0.62)	1.73 (0.51)	5.88 (0.24)		4.63 (0.33)
$H_3PO_4^0$	10.03 (0.05)	2.06 (0.17)	2.16 (0.62)		1.71 (0.62)	1.76 (0.48)	5.76 (0.25)		4.47 (0.35)
$H_3SiO_4^{1-}$	10.04 (0.04)	2.06 (0.17)	2.17 (0.60)		1.73 (0.60)	1.70 (0.49)	5.77 (0.25)		4.47 (0.34)
$H_4SiO_4^0$	10.05 (0.04)	2.05 (0.17)			1.83 (0.60)	1.75 (0.49)			4.36 (0.36)
$HBrO_4^0$	27.79 (0.04)	2.04 (0.17)			1.07 (0.80)	1.79 (0.49)	8.00 (0.19)	7.97 (0.19)	5.20 (0.31)
$HSeO_4^{1-}$	27.85 (0.04)	2.05 (0.17)			0.93 (0.79)	1.76 (0.49)	7.96 (0.17)	7.96 (0.17)	5.36 (0.31)
$HAsO_4^{2-}$	27.85 (0.04)	2.05 (0.17)			0.97 (0.76)	1.75 (0.51)	7.98 (0.16)	7.91 (0.15)	5.32 (0.31)
$HGeO_4^{3-}$	27.83 (0.04)	2.06 (0.17)			0.72 (0.81)	1.78 (0.51)	7.94 (0.16)	7.88 (0.16)	5.56 (0.30)
$H_2SeO_4^0$	27.80 (0.04)	2.06 (0.17)			0.71 (0.82)	1.78 (0.49)	7.97 (0.18)		5.53 (0.32)
$H_2AsO_4^{1-}$	27.81 (0.04)	2.05 (0.17)			0.80 (0.79)	1.75 (0.49)	7.96 (0.16)		5.48 (0.32)
$H_2GeO_4^{2-}$	27.82 (0.04)	2.06 (0.17)			0.79 (0.79)	1.75 (0.51)	7.88 (0.15)		5.55 (0.30)
$H_3AsO_4^0$	27.85 (0.04)	2.05 (0.17)				1.76 (0.49)	8.00 (0.16)		6.23 (0.27)
$H_3GeO_4^{1-}$	27.83 (0.04)	2.05 (0.17)			0.67(0.81)	1.73 (0.49)	7.96 (0.15)		5.59 (0.30)
$H_4GeO_4^0$	27.83 (0.04)	2.06 (0.17)				1.75 (0.49)			6.23 (0.25)

[a] Values of $\bar{N}$ are electronic populations. [b] Synaptic valence basins of protonated oxygens.

VSCC along X−O(H) bond paths (Figure 1). The VSCC closest to O on the bond path has AIM properties similar to two other VSCC of oxygen pointing outward from the molecule. This VSCC is, however, not associated with a (3,−3) critical point of $\eta(r)$ and is therefore not an attractor in its own right, but it does underscore an important charge transfer to O.

P-containing oxyanions have additional VSCC outside X−O bond paths that could suggest other bonding schemes. In HPO_4^{1-}, three VSCC are in trigonal symmetry about the P−OH axis (shown as solid gray circles in Figure 1) and the three others are at the antipodes of P (shown as solid black circles). These VSCC have, however, small values of $\rho = 0.05$ au and $-\nabla^2\rho = 0.07$ and are not recovered as maxima in $\nabla\eta(r)$. The same holds for the five VSCC in $H_2PO_4^{1-}$, with nearly identical AIM properties. The P−O bond in $H_3PO_4^0$ has three VSCC in trigonal symmetry about the axis that are closely related to three (3,−

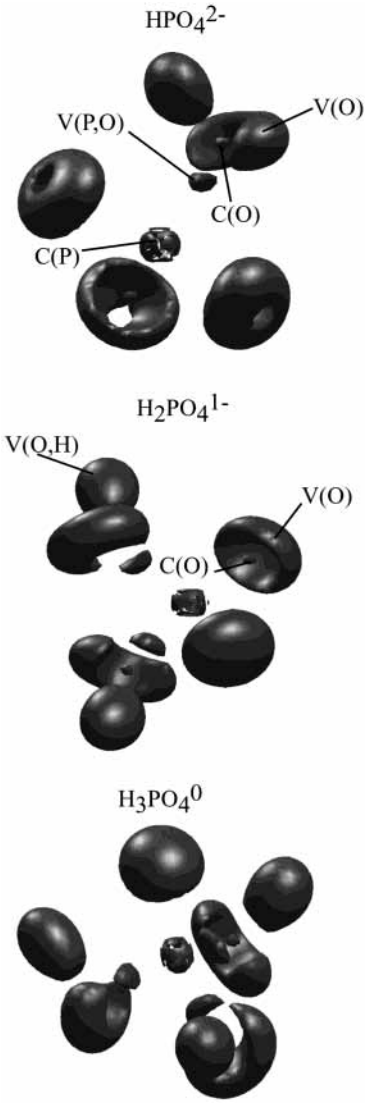

Figure 4. Typical ELF localization domains for HPO_4^{2-}, $H_2PO_4^{1-}$, and $H_3PO_4^{\circ}$ at isosurfaces of $\eta(r) = 0.85$.

3) critical points of $\eta(r)$. These attractors correspond to three highly correlated V(P,O) basins with about 0.7*e* ($\lambda = 0.81$) each. Once coalesced to one superbasin, the population of 2.16*e* ($\lambda = 0.62$) may suggest a slight contribution of π bonding but the distribution of electrons remains highly isotropic, given the near-zero values of ϵ. The same observations also hold for the Si−O bond in $H_3SiO_4^{1-}$. P−O and Si−O bonds have also the largest angles $\angle$ X−O−VSCC of 126.8° and 140.0°, respectively, showing that the shorter bonds repel the most V(O) basin electrons. Their associated V(X,O) populations of 2.16−2.17*e* and their correlative V(O) populations of about 5.76−5.77*e* thus suggest that even the shortest distances are chiefly explained by shared σ bonds.

3.3. The Nature of O−H Bonds. *AIM Analysis.* The properties of the (3,−1) bond critical points of O−H bonds are reported in Table 2, and all have properties close to those previously described for hydroxyls.[5] All bonds have (1) distances ranging from 0.960 to 0.975 Å, (2) values of $\rho(r_c)$ from 0.351 to 0.365 au, (3) values of $\nabla^2\rho(r_c)$ from −2.532 to −2.419 au, and (4) $\lambda_1/\lambda_3 \gg 1$, $G(\rho(r_c))/\rho(r_c) \ll 1$, and $E_e(r_c) \ll 1$. The bond is therefore typical of shared interactions, with insignificant values of ϵ, ranging from 0.004 to 0.018. The absence of (3,−1) bond critical points between H and neighboring O atoms also show the lack of intramolecular hydrogen bonding. Protons are thus likely to be oriented by the negative charge of nonbonding electrons of neighboring O without, however, resulting in an interpenetration of van der Waals radii.[5]

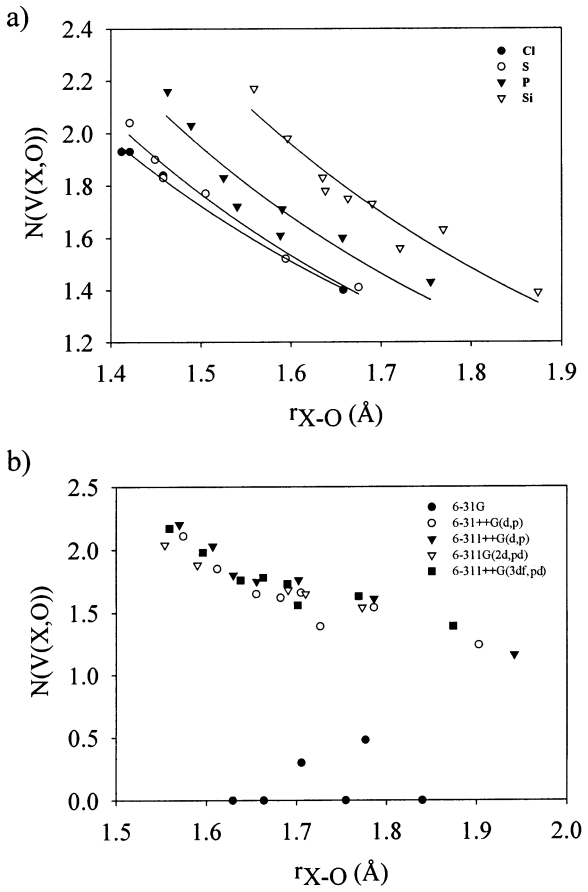

Figure 5. Disynaptic basin population (*e*) as a function of X−O bond length for (a) 3rd-row oxyacids and oxyanions[10] at the B3LYP/6-311++G(3df,pd) level, and (b) for H_2SiO_4 ($z = 0$ to 4) with different basis sets.

ELF Analysis. All V(O,H) basin populations range from 1.70 to 1.79*e* and have similar values of delocalization ($\lambda = 0.48-0.51$) with strong cross-contributions with their respective V(O) basins. The basin populations are larger for species of lower protonation level and of larger charge; for example, among HXO_4 anions, $\bar{N}$ tends to decrease in the order Cl > S > P > Si and Br > Se > As > Ge. Values of $\bar{N}$ are also larger in longer O−H bonds. These trends are, however, the result of only small variations, and in a global sense the bonding nature and electronic population of O−H bonds in all oxyacids can be said to be insensitive to the nature of X−O bonds.

3.4. Acidities. G2-calculated gas-phase enthalpies of acidity are reported in Table 4. The values for $HClO_4^0$, $H_2SO_4^0$, and $H_3PO_4^0$ compare well with the few experimental values available.[38] Aqueous-phase pK_a's also correlate well with G2-calculated values (Figure 6a), despite expected effects from solvent interactions[39] (illustrated for, for example, oxyacids[12−14] and superacids[40]). Figure 6b also shows that G2-calculated enthalpies of acidity correlate well with ab initio molecular electrostatic potentials at H sites (Table 4). Various attempts have previously been made to apply simple electrostatic models to predict acidity[12,13] using point charges condensed to nucleic coordinates (e.g., natural bond order charges[13] and electrostatic

TABLE 4: G2-Calculated $\Delta_{acid(g)}H^0_{298}$ (kJ/mol) (G2), pK_a's, and Electrostatic Potentials (kJ/mol) at H^+ Sites for Neutrally- and Singly-Charged Oxyacids

	$\Delta_{acid(g)}H^0_{298}$	p$K_{a(exp)}$[g]	$V(H^+)$
$HBrO_4^0$	1229.9		−2364.2
$HClO_4^0$	1246.5[a]	(−7)[e]	−2366.3
$H_2SeO_4^0$	1291.8		−2405.0
$H_2SO_4^0$	1297.2[b,c]	(−1.98)[f]	−2394.5
$H_3AsO_4^0$	1360.5	2.24	−2474.0
$H_3PO_4^0$	1366.2[d]	2.15	−2464.5
$H_4GeO_4^0$	1457.6	9.3	−2567.8
$H_4SiO_4^0$	1470.0	9.86	−2564.9
$HSeO_4^{1-}$	1828.0	1.7	−2979.8
HSO_4^{1-}	1867.4	1.99	−3002.8
$H_2AsO_4^{1-}$	1880.3	6.96	−3024.6
$H_2PO_4^{1-}$	1909.3	7.2	−3033.2
$H_3GeO_4^{1-}$	1927.3	12.6	−3079.3
$H_3SiO_4^{1-}$	1953.6	13.1	−3086.6

[a] Experimental result:[48] 1200 kJ/mol. [b] Experimental result:[49] 1282±13 kJ/mol. [c] Experimental result[50]:1295±11 kJ/mol. [d] Experimental result:[51] 1382±21 kJ/mol. [e] Estimate taken from ref 13. [f] Estimate taken from ref 52. [g] All pK_a's are taken from refs 45−47 and hold for an ionic strength of $I = 0$ at 298.15 K.

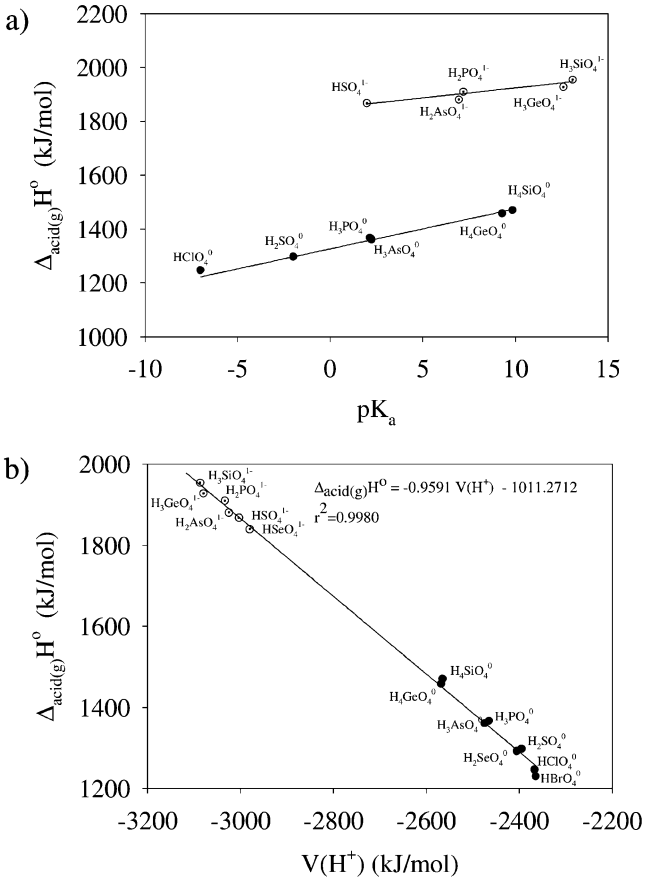

Figure 6. G2-calculated enthalpies of acidity (a) as a function of pK_a's for neutrally- and singly-charged oxyacids, and (b) as a function of the electrostatic potential at the site of protons calculated at the B3LYP/6-311++G(3df,pd) level.

potential-derived point charges). Merz−Singh−Kollman[10] charges were calculated for the oxyacids considered in this study (not reported here) but, much like the results of similar studies,[13,42] relationships with calculated gas-phase enthalpies of acidities or with pK_a's are ambiguous. Good correlations have also been reported for nitrogen and phosphorus bases with the properties of $\nabla^2\rho(r_c)$[41] and one-electron potentials.[42] The electronic population of monosynaptic basins of basic moieties was also proposed as part of a rationalizing tool to predict protonation sites in bases.[43] In all these cases, intramolecular distributions of electrons are determining in understanding acidity. In the simpler application of underbonding, intramolecular distributions of electrons are obtained from semiempirical actual bond valences.[2] As ELF domains provide an explicit notion of intramolecular distribution in terms of electron populations, these will here be used to test the concept of underbonding by considering populations in conjugate acids and bases of main-group oxyacids.

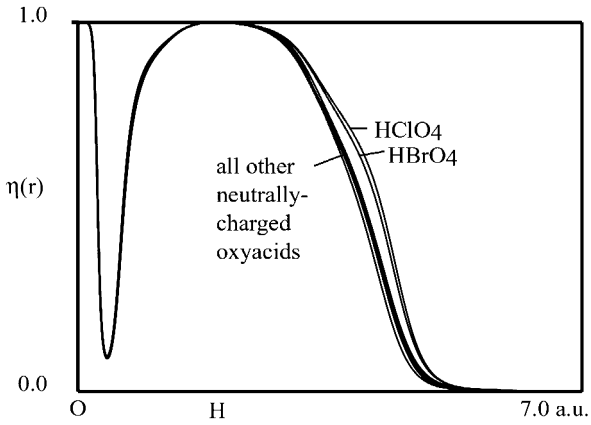

Figure 7. Values of $\eta(r)$ along the O−H axis in all neutrally-charged 3rd- and 4th-row main-group oxyacids considered in this study (B3LYP/6-311++G(3df,pd)).

Classic explanations of acidity invoke the interplay of electronegativity and molecular size, whereby the electron-withdrawing capability of a base competes with the increased delocalization of electrons on larger-sized bases (e.g., the trend in increasing acidity in Group 16 H_2X molecules). The concept of electron withdrawal is specifically taken into account in the concept of underbonding. In the case of oxyacids, a center X is expected to withdraw a given number of electrons from the valence shell of oxygen and thereby tap into the pool of electrons available for stabilizing O−H bonds. Results of the ELF analyses, however, show that this may be otherwise. Indeed, V(O,H) basin populations not only are limited to a very narrow range (1.70 to 1.79*e*) but also are larger for longer O−H bonds and larger for stronger acids, a counterintuitive result also encountered in hypophalous acids.[44] Moreover, profiles of $\eta(r)$ along O−H bonds in all neutrally-charged oxyacids, shown in Figure 7, confirm the insensitivity of these results on acid strength, save the two slight outlying curves for $HClO_4^0$ and $HBrO_4^0$. There is, therefore, no significant positive correlation between V(O,H) populations and the large range of acid strengths in main-group oxyacids. Likewise, the variance on the electronic population of V(O), here quantified through the relative fluctuation (eq 6), fails at providing any clear trends in acidity through the concept of electron delocalization.

In contrast to the largely insensitive V(O,H) basin populations, those of V(O) and V(X,O(H)) undergo more dramatic changes. We first note that the exponential relationships between 3rd-row V(X,O(H)) electronic populations and X−O bond length have also been reported for $\rho(r_c)$[32−36] (Figure 5) and with actual bond valences[2], i.e., the value used to quantify underbonding. We, however, note that while values of $\rho(r_c)$ for a given X−O distance are larger for centers X of larger electronegativity, those of V(X,O(H)) basin populations show the opposite trend. Some reconciliation to this counterintuitive observation can, however, be found in the following observations.

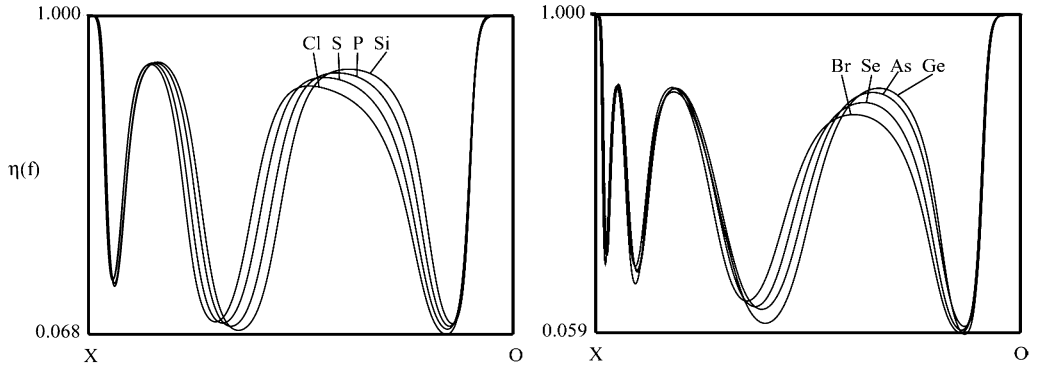

Figure 8. Values of $\eta(r)$ along the X−O axis of all neutrally-charged 3rd- and 4th-row main-group oxyacids (B3LYP/6-311++G(3df,pd)). The abscissa is normalized for each oxyacid-specific X−O bond length.

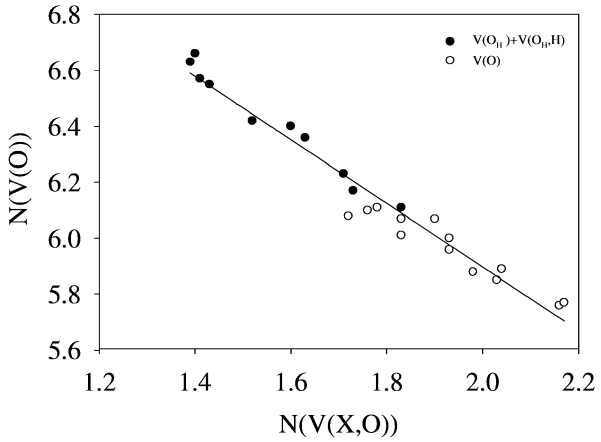

Figure 9. Electronic populations of monosynaptic and protonated disynaptic basins of O as a function of those X−O disynaptic basins in all 3rd-row main-group oxyacids considered in this study (B3LYP/6-311++G(3df,pd)). This relationship cannot be shown for 4th-row oxyacids due to the constant V(O) population of about 7.88−8.00*e*.

(1) Values of $\eta(r)$ along the X−O axis (Figure 8) reach a maximum closer to X in the order Si < P < S < Cl, i.e., with increasing electronegativity.

(2) The volumes of V(X,O) basins, v (not reported here), decrease in the order Si > P > S > Cl, i.e., with decreasing X−O bond length. The volume of a V(Si,O) basin, for example, is about $^5/_3$ times larger than that of a V(Cl,O) basin of equal electronic population.

(3) The mean electronic density of V(X,O) basins, $\bar{\rho} = \bar{N}/v$ (not reported here), increases in the order Si < P < S < Cl and is constant for any given X. The mean electronic density of any V(Si,O) basin, for example, is about $^3/_2$ times smaller than any V(Cl,O) basin of equal volume.

The electronegativity of X thus controls the approach of $\eta(r)$ maxima and values of $\bar{\rho}$ in V(X,O) basins. The population of V(X,O) basins, however, result from the interplay of $\bar{\rho}$ and X−O bond length: oxyanions with X of smaller electronegativity but of larger disynaptic basin volumes may thus have larger values of $\bar{N}$ of although low $\bar{\rho}$. In addition, recalling the relationship shown in Figure 5a, it should be noted that within a class of oxyanions of center X a protonation-induced increase in X−OH bond length will result in a decrease in volume and $\bar{N}$(V(X, O)), thereby increasing $\bar{N}$(V,O)). This redistribution of electrons is also reflected by a linear relationship between V(X,O) and V(O(H)) populations shown in Figure 9, but has no apparent relationship to acidity. Moreover, as 4th-row oxyanion V(O) basins all possess about 7.88−8.00*e*, i.e., irrespective of their acid strengths, V(O) basins populations cannot be a general rationalizing argument for acidity of these main-group oxyacids. The concept of underbonding may therefore warrant further investigations.

4. Summary

AIM and ELF analyses have shown X−O(H) bonds to be characteristic of σ-bonded shared interactions in 3rd-row oxyacids but of σ-bonded closed-shell interactions in their 4th-row counterparts and to have nonbonded electron populations resulting from the nature of X−O bonds. These important differences do not, however, affect acidity trends among same-group homologous molecules. The results of the ELF analyses do not support underbonding as a rationalizing argument for trends in acidity. In fact, trends in gas-phase enthalpies of acidity and pK_a's are better described with the electrostatic potential at the site of the proton.

Acknowledgment. This work was supported by the Swiss Federal Institute of Technology (ETH-Zürich). The Competence Centre for Computational Chemistry (C4) at ETH-Zürich is thanked for providing access and support to its facilities.

References and Notes

(1) Pauling, L. *J. Am. Chem. Soc.* **1929**, *51*, 1010.
(2) Brown, I. D.; Altermatt, D. *Acta Crystallogr. B* **1985**, *41*, 244.
(3) Hiemstra, T.; Venema, P.; van Riemsdijk, W. H. *J. Colloid Interface Sci.* **1996**, *179*, 488.
(4) Rietra, R. J. J.; Hiemstra, T.; van Riemsdijk, W. H. *Geochim. Cosmochim. Acta* **1999**, *63*, 3009.
(5) Bader, R. F. W. *Atoms In Molecules: A Quantum Theory*; Clarendon Press: Oxford, U.K., 1990.
(6) Silvi, B.; Savin, A. *Nature* **1994**, *371*, 683.
(7) Becke, A. D.; Edgecombe, K. E. *J. Chem. Phys.* **1990**, *92*, 5397.
(8) Boily, J.-F. *J. Phys. Chem. A* **2002**, *106*, 4718.
(9) Mulliken, R. S. *J. Chem. Phys.* **1955**, *23*, 1833.
(10) (a) Sing, U. C.; Kollman, P. A. *J. Comput. Chem.* **1984**, *5*, 129. (b) Besler, B. H.; Merz, K. M.; Kollman, P. A. *J. Comput. Chem.* **1990**, *11*, 431.
(11) (a) Curtiss L. A.; Raghavachari, K.; Trucks, G. W.; Pople, J. A. *J. Chem. Phys.* **1991**, *94*, 7221. (b) Curtiss, L. A.; McGrath, M. P.; Blaudeau, J.-P.; Davis, N.; Binning, E. R. C. J.; Radom, L. *Am. Inst. Phys.* **1995**, *103*, 6104.
(12) Sefčik, J.; Goddard, W. A., III. *Geochim. Cosmochim. Acta* **2001**, *65*, 4435.
(13) Tossell, J. A.; Sahai, N. *Geochim. Cosmochim. Acta* **2000**, *64*, 4097.
(14) Rustad, J. R.; Dixon, D. A.; Kubicki, J. D.; Felmy, A. R. *J. Chem. Phys. A* **2000**, *104*, 4051.
(15) Venema. P.; Hiemstra, T.; Weidler, P. G.; van Riemsdijk, W. H. *J. Colloid Interface Sci.* **1998**, *198*, 282.
(16) Lewis, G. N. *J. Am. Chem. Soc.* **1916**, *38*, 762.
(17) Lewis, G. N. *J. Am. Chem. Soc.* **1933**, *1*, 17.
(18) Savin, A.; Jepsen, O.; Flad, J.; Andersen, O. L.; Preuss, H.; von Schnering, J. G. *Angew. Chem., Int. Ed. Engl.* **1992**, *31*, 187.
(19) Savin, A.; Silvi, S.; Colonna, F. *Can. J. Chem.* **1996**, *74*, 1088.
(20) Noury, S.; Krokidis, X.; Fuster, F.; Silvi, B. *Comput. Chem.* **1999**, *23*, 597.

(21) Noury, S.; Colonna, N.; Savin, A.; Silvi, B. *J. Mol. Struct.* **1998**, *450*, 59.
(22) (a) Becke, A. D. *J. Chem. Phys.* **1993**, *98*, 5648. (b) Lee, C.; Yang, W.; Parr, R. G. *Phys. Rev. B* **1988**, *37*, 785.
(23) Frisch, M. J.; Trucks, G. W.; Schlegel, H. B.; Scuseria, G. E.; Robb, M. A.; Cheeseman, J. R.; Zakrzewski, V. G.; Montgomery, J. A., Jr.; Stratmann, R. E.; Burant, J. C.; Dapprich, S.; Millam, J. M.; Daniels, A. D.; Kudin, K. N.; Strain, M. C.; Farkas, O.; Tomasi, J.; Barone, V.; Cossi, M.; Cammi, R.; Mennucci, B.; Pomelli, C.; Adamo, C.; Clifford, S.; Ochterski, J.; Petersson, G. A.; Ayala, P. Y.; Cui, Q.; Morokuma, K.; Malick, D. K.; Rabuck, A. D.; Raghavachari, K.; Foresman, J. B.; Cioslowski, J.; Ortiz, J. V.; Stefanov, B. B.; Liu, G.; Liashenko, A.; Piskorz, P.; Komaromi, I.; Gomperts, R.; Martin, R. L.; Fox, D. J.; Keith, T.; Al-Laham, M. A.; Peng, C. Y.; Nanayakkara, A.; Gonzalez, C.; Challacombe, M.; Gill, P. M. W.; Johnson, B. G.; Chen, W.; Wong, M. W.; Andres, J. L.; Head-Gordon, M.; Replogle, E. S.; Pople, J. A. *Gaussian 98*, revision A.11.1; Gaussian, Inc.: Pittsburgh, PA, 1998.
(24) Seeger, R.; Pople, J. A. *Chem. Phys.* **1977**, *66*, 3045.
(25) Bauernschmitt, R.; Ahlrichs, R. *J. Chem. Phys.* **1996**, *104*, 9047.
(26) Johnson, B. G.; Gill, P. M. W.; Pople, J. A. *Chem. Phys. Lett.* **1993**, *206*, 239.
(27) MORPHY98 is a program written by P. L. A. Popelier with a contribution from R. G. A. Bone, UMIST, Manchester, England, EU, 1998.
(28) Gal, J.-F. *J. Mass Spectrom.* **1999**, *23*, 597.
(29) Mills, I.; Cvitas, T.; Homann, K.; Kallay, N.; Kuchitsu, K. *Quantities, Units and Symbolism in Physical Chemistry*, 2nd ed.; Blackwell Science: Oxford, 1993.
(30) (a) G2 in Gaussian98 also includes an implementation for non-transition 3rd-row elements. (b) Curtiss L. A.; Raghavachari, K.; Trucks, G. W.; Pople, J. A. *J. Chem. Phys.* **1991**, *94*, 7221. (c) Curtiss, L. A.; McGrath, M. P.; Blaudeau, J.-P.; Davis, N.; Binning, E. R. C. J.; Radom, L. *Am. Inst. Phys.* **1995**, *103*, 6104.
(31) See references in ref 8.
(32) Gibbs, G. V.; Hill, F. C.; Boisen, M. B., Jr. *Phys. Chem. Miner.* **1997**, *24*, 167.
(33) Hill, F. C.; Gibbs, G. V.; Boisen, M. B., Jr. *Phys. Chem. Miner.* **1997**, *24*, 582.
(34) Gibbs, G. V.; Hill, F. C.; Boisen, M. B.; Downs, R. T. *Phys. Chem. Miner.* **1998**, *25*, 585.
(35) Gibbs, G. V.; Boisen, M. B.; Hill, F. C.; Tamada, O.; Downs, R. T. *Phys. Chem. Miner.* **1998**, *24*, 574.
(36) Gillespie, R. J.; Bytheway, I.; Robinson, E. A. *Inorg. Chem.* **1998**, *37*, 2811.
(37) Krokidis, X.; Noury, S.; Silvi, B. *J. Phys. Chem. A* **1997**, *101*, 7277.
(38) cf. http://webbook.nist.gov.
(39) Reichardt, C. *Solvents and Solvent Effects in Organic Chemistry*, 2nd ed.; VCH: Weinheim, 1988.
(40) Koppel, I. A.; Burk, P.; Koppel, I.; Leito, I.; Sonoda, T.; Mishima, M. *J. Am. Chem. Soc.* **2000**, *122*, 5114.
(41) Tang, T.-H.; Hu, W.-J.; Yan, D.-Y.; Cui, Y.-P. *J. Mol. Struct. (THEOCHEM)* **1990**, *207*, 327.
(42) Chan, W.-T.; Hamilton, I. P. *Chem. Phys. Lett* **1999**, *301*, 53.
(43) Fuster, F.; Silvi, B. *Chem. Phys.* **2000**, *252*, 279.
(44) Berski, S.; Silvi, B.; Latajka, Z.; Leszczyński, J. *J. Chem. Phys.* **1999**, *111*, 2542.
(45) Smith, R. M.; Martell, A. E. *Critical Stability Constants. Volume 4: Inorganic Complexes*; Plenum Press: New York, 1976.
(46) Smith, R. M.; Martell, A. E. *Critical Stability Constants. Volume 5: First Supplement*; Plenum Press: New York, 1982.
(47) Smith, R. M.; Martell, A. E. *Critical Stability Constants. Volume 6: Second Supplement*; Plenum Press: New York, 1989.
(48) Marcus, Y. *J. Chem. Soc., Faraday Trans I* **1987**, *83*, 339.
(49) Wang, X. B.; Nicholas, J. B.; Wang, L. S. *J. Phys. Chem. A* **2000**, *104*, 504.
(50) Viggiano, A. A.; Henchmann, M. J.; Dale, F.; Deakyne, C. A.; Paulson, J. F. *J. Am. Chem. Soc.* **1992**, *114*, 4299.
(51) Morris, R. A.; Knighton, W. B.; Viggiano, A. A.; Hoffman, B. C.; Schaefer, H. F., III. *J. Phys. Chem. A* **1997**, *106*, 3545.
(52) Hiemstra, T.; van Riemsdijk, V. H.; Bolt, G. H. *J. Colloid Interface Sci.* **1989**, *133*, 91.